PERGAMON

Polyhedron 21 (2002) 1779–1786

POLYHEDRON

www.elsevier.com/locate/poly

A tetranuclear manganese carboxylate cluster with bis(2-pyridyl)amine ligation: $[Mn_4O_2(O_2CEt)_7(bpya)_2](ClO_4)$

Guillem Aromí [a], Sumit Bhaduri [a], Pau Artús [a], John C. Huffman [a], David N. Hendrickson [b], George Christou [a,*]

[a] Department of Chemistry and the Molecular Structure Center, Indiana University, Bloomington, IN 47405-7102, USA
[b] Department of Chemistry and Biochemistry-0358, University of California at San Diego, San Diego, La Jolla, CA 92093-0358, USA

Received 8 January 2002; accepted 1 May 2002

Abstract

The title complex has been prepared and characterized by X-ray crystallography, magnetochemistry, cyclic voltammetry and ^{1}H NMR spectroscopy. The complex contains a $[Mn_4(\mu_3\text{-}O)_2]^{8+}$ core with bridging $EtCO_2^-$ and chelating bpya groups. The magnetochemical studies indicate an $S = 0$ ground state as a result of antiferromagnetic exchange interactions between the Mn^{III} ions. The ^{1}H NMR spectra support retention of the solid-state structure on dissolution in MeCN. © 2002 Elsevier Science Ltd. All rights reserved.

Keywords: X-ray crystallography; Magnetochemical studies; Manganese oxide clusters

1. Introduction

The current interest in the synthesis of new manganese oxide clusters has two main driving forces: (i) the desire to recreate with synthetic models the structure and/or properties of the active site of metalloenzymes containing an oxide-bridged manganese core such as the water oxidizing complex of Photosystem II and the catalase enzymes [1]; and (ii) the realization that manganese oxide clusters often exhibit high spin ground states as a result of ferromagnetic exchange interactions and/or spin frustration effects [2–11]. In addition, such clusters have provided the first examples of single molecules that can be magnetized below a certain temperature [2–5,12–17], for which the term single-molecule magnet has been recently coined [4].

We and others have employed the coordinating versatility of carboxylate groups, often in combination with other ligands, to generate a number of manganese clusters with a large range of nuclearities and topologies [2–4,7–9,18–26]. As part of continuing efforts to prepare new members of this family, we have investigated the reactions of bis(2-pyridyl)amine (bpya) with Mn complexes. There are no structures of Mn compounds in the literature containing this ligand, which is usually seen as a chelate in mononuclear species, particularly with Cu [27–29], and a few dinuclear Cu species [30,31]. In addition, a number of linear trimetallic arrays held together by bpya in its deprotonated form have been reported [32–34].

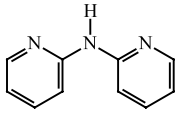

We herein describe the preparation, crystal structure, and properties of the complex $[Mn_4O_2(O_2CEt)_7(bpya)_2](ClO_4)$ (**1**), which possesses a butterfly-like $[Mn_4O_2]$ core. The influence that the significantly strained chelate exerts on the magnetic properties of this cluster is discussed, in relation to previously reported complexes with a similar core [35–39].

* Corresponding author. Present address: Department of Chemistry, University of Florida, Gainesville, FL 32611-7200, USA. Tel./fax: +1-812-855-2399
E-mail address: christou@indiana.edu (G. Christou).

0277-5387/02/$ - see front matter
PII: S0277-5387(02)01040-9

2. Experimental

2.1. Materials and methods

All manipulations were performed under aerobic conditions using materials as received, except where indicated otherwise. $NBu^n_4MnO_4$ was prepared as described elsewhere [46], $[Mn_3O(O_2CEt)_6(py)_3](ClO_4)$ was available from previous work [47].

2.2. Syntheses

2.2.1. $Mn(O_2CEt)_2\cdot 0.35H_2O$

To a slurry of $MnCO_3$ (30 g, 0.26 mol) in water (200 mL) was added dropwise propionic acid (25 ml, 0.33 mol). The mixture was stirred for a few days and the unreacted $MnCO_3$ was removed by filtration. The pale brown filtrate was roto-evaporated to dryness to yield a pink solid. The yield was 79%. *Anal.* Calc. (Found) for $Mn(O_2CEt)_2\cdot 0.35H_2O$: C, 34.75 (34.51); H, 5.20 (4.89); N, 0.00 (0.00)%.

2.2.2. $[Mn_4O_2(O_2CEt)_7(bpya)_2](ClO_4)\cdot 2EtCO_2H$ (**1**)

A solution of $Mn(O_2CEt)_2\cdot 0.35H_2O$ (757 mg, 3.65 mmol) in water (6 ml) was added to a solution of bpya (356 mg, 2.08 mmol) and NBu_4ClO_4 (520 mg, 1.52 mmol) in propionic acid (25 ml). To the resulting yellow solution was added dropwise a solution of $NBu^n_4MnO_4$ (0.27 g, 0.70 mmol) in MeCN (2 ml) to yield a red solution, which was stirred for ~ 3 h. Addition of Et_2O (200 ml) led to precipitation of a microcrystalline red product that was collected by filtration, washed with Et_2O and dried in vacuo. The yield was 68% based on total available Mn. *Anal.* Calc. (Found) for **1**·2Et-CO_2H: C, 41.72 (41.71); H, 4.84 (4.84); N, 6.21 (6.14)%. To a saturated solution of **1** in MeCN was added toluene (approximately one-fourth of the solution volume) and the mixture left to slowly evaporate at room temperature (r.t.). Crystals suitable for X-ray crystallography deposited over two weeks.

2.3. Crystal structure of *1*

Data were collected on a Bruker Smart 6000 CCD system with a sealed molybdenum source and graphite monochromator. Small crystals were selected from the bulk sample and transferred to the goniostat where they were cooled to −160 °C for data collection and characterization. The data were collected using 10 s frames with an omega scan of 0.30° and corrected for Lorentz and polarization effects. Equivalent reflections were averaged using the Bruker SAINT software, as well as utility programs from the XTEL library ($R_{av} = 0.076$). The space group was *Pbca*. The structure was readily solved using SHELXTL and Fourier techniques. Many of the hydrogen atoms were visible in a difference Fourier map phased on the non-hydrogen atoms. All hydrogen atoms were placed in idealized, calculated positions and treated as fixed atom contributors in the final cycles of refinement. The structure was well ordered with the exception of one $EtCO_2^-$ ligand in which the methyl group was disordered (C47). The MeCN solvent was also found to be in 50% occupancy. A final difference Fourier map was essentially featureless, the largest peak being 0.83 e A^{-3}. The final $R(R_w)$ indices were 3.72(3.92) using 5341 independent reflections with $I > 2.33\sigma(I)$. Crystallographic data are summarized in Table 1.

2.4. Other measurements

^1H NMR spectra were collected on a 300 MHz Varian Gemini 2000 spectrometer and a 500 MHz Varian Inova spectrometer with the protio-solvent signal used as reference. Chemical shifts are quoted on the δ scale (downfield shifts are positive). Cyclic voltammetry was performed in MeCN solution using 0.1 M NBu_4PF_6 as supporting electrolyte using a BAS CV-50 voltammetric analyzer. Electrodes were a glassy carbon working electrode, a platinum wire auxiliary electrode, and a silver wire in a 1 M $AgNO_3$ MeCN solution, connected to the cell solution through a saline bridge, as reference electrode. Dc magnetic susceptibility data were collected on powdered, microcrystalline samples (restrained in eicosane to prevent torquing) with a Quantum Design MPMS-XL SQUID magnetometer equipped with a 5.5 T (55 kG) magnet. A diamagnetic correction to the observed susceptibilities was applied using Pascal's constants. Elemental analyses were performed by Atlantic Microlab.

Table 1
Crystallographic data for $[Mn_4O_2(O_2CEt)_7(bpya)_2](ClO_4)\cdot MeCN$ (**1**)

Formula [a]	$C_{43}H_{56}ClMn_4N_7O_{20}$
F_W (g mol^{-1})	1234.15
Space group	*Pbca*
Unit cell dimensions	
a (Å)	23.880(3)
b (Å)	18.019(2)
c (Å)	25.191(3)
V (Å^3)	10839.58
Z	8
T (°C)	−160
Radiation [b] (Å)	0.71069
ρ_{calc} (g cm^{-3})	1.513
μ (cm^{-1})	10.376
R [c] (%)	3.72
R_w [d] (%)	3.92

[a] Including solvate molecules.
[b] Mo Kα, graphite monochromator.
[c] $R = 100\ \Sigma\ ||F_o| - |F_c||/\Sigma\ |F_o|$.
[d] $R_w = 100\ [\Sigma\ w(|F_o| - |F_c|)^2/\Sigma\ w|F_o|^2]^{1/2}$ where $w = 1/\sigma^2(|F_o|)$.

3. Results and discussion

3.1. Synthesis and reactivity

We have recently prepared a number of $Mn_x/O/RCO_2$ aggregates using comproportionation reactions between $Mn(O_2CR)_2$ (R = Me, Et) and MnO_4^- in the presence of a chelating ligand and the corresponding carboxylic acid. This route has provided convenient access to various tetranuclear Mn complexes with trigonal pyramidal or butterfly-like Mn_4 topologies [40]. When $NBu^n_4MnO_4$ in MeCN was added to $Mn(O_2CEt)_2$ in $EtCO_2H/H_2O$ (5:1 v/v) in the presence of bpya and $NBu^n_4ClO_4$, a dark red solution was obtained from which $[Mn_4O_2(O_2CEt)_7(bpya)_2](ClO_4)$ (**1**) was obtained in high yield as a red microcrystalline solid upon addition of Et_2O. The reaction is summarized in Eq. (1).

$$16Mn(O_2CEt)_2 + 4MnO_4^- + 10bpya + 12EtCO_2H \rightarrow 5[Mn_4O_2(O_2CEt)_7(bpya)_2]^+ + 9EtCO_2^- + 6H_2O \quad (1)$$

The crystal structure of **1** (vide infra) shows that bpya is bound in its neutral form, consistent with the acidic conditions of the reaction medium. Since this ligand has been found chelating as a deprotonated anion in a few cases [43,44], the question arose whether under different conditions lacking added acid the ligand would appear in a deprotonated form. The reaction of preformed trinuclear complexes $[Mn_3O(O_2CR)_6(L)_3]^{0,+}$ (L = py, H_2O) with chelating ligands has been used extensively in the past to trigger structural rearrangements leading to higher nuclearity products [45]. With this in mind, the reaction of $[Mn_3O(O_2CEt)_6(py)_3](ClO_4)$ with bpya was investigated. A dark brown solution of the trinuclear complex in MeCN was treated with 1.5 equiv. of bpya, and a red-brown precipitate started to form within minutes. This product was identified as predominantly complex **1** by IR and ^1H NMR spectroscopy.

3.2. Description of the structure of *1*

Crystallographic data for $[Mn_4O_2(O_2CEt)_7(bpya)_2](ClO_4)$ (**1**) are listed in Table 1. A labeled ORTEP representation of the cation of complex **1** is presented in Fig. 1, and selected interatomic distances and bond angles are listed in Table 2. The core consists of four Mn ions bridged by two μ_3-oxide ions, the ensemble having a butterfly-like topology. Approximately octahedral coordination around each Mn(III) is completed by the peripheral ligation, comprising seven μ_2-O_2CEt^- groups and two bpya ligands. One carboxylate is bound only to 'body' Mn ions, Mn2 and Mn3, while each of the other six is bridging a body-wingtip Mn_2 pair. The bpya groups chelate the two wingtip Mn ions Mn1 and Mn4. The cluster possesses virtual C_2 symmetry. Charge considerations indicate the oxidation state +3 for all four metals, as confirmed by the presence of a Jahn–Teller elongation of two *trans* bonds (av. 2.138 Å) at each Mn center, although the equatorial bond distances span a wide range (1.833–2.087 Å). The Mn_4O_2 core contains four different types of Mn···Mn vectors: Mn2 and Mn3 are 2.871(2) Å apart, the body Mn ions are separated from the wingtip ions by averages of 3.307 Å (two carboxylate bridges) and 3.444 Å (one carboxylate bridge), and the Mn1···Mn4 distance is 5.834 Å. The overall structure of this molecule is similar to that of other previously reported clusters with the $[Mn_4O_2]^{8+}$ core [36–40,47] (vide infra), but is the first with a six-membered N-based chelate ring. These six-membered chelate rings are in a boat conformation, as commonly seen for bpya although the extent of the folding varies greatly from compound to compound. The factors determining the exact shape of the chelate ring seem to be mainly steric and possibly involve crystal packing forces as well. The folding of the boat is gauged by the angles between the least-squares plane defined by N_a, N_b, C_b and C_a, and the planes C_a–N_c–C_b and N_a–Mn–N_b, averaging 23.79 and 28.97°, respectively, for complex **1**.

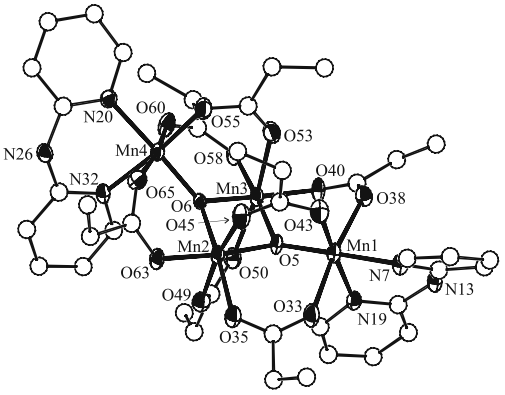

Fig. 1. ORTEP representation of the cation of $[Mn_4O_2(O_2CEt)_7(bpya)_2](ClO_4)$ at the 50% probability level (carbons represented isotropically).

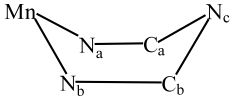

3.2.1. Comparison of *1* with other $[Mn_4O_2]^{8+}$ complexes

As stated above, complex **1** is a new addition to the family of Mn clusters with the butterfly-like $[Mn_4O_2]^{8+}$ core, enlarging the available database of such complexes for identifying correlations between structure and physico-chemical properties. In Table 3 is presented a comparison between the core parameters of **1** and those of $[Mn_4O_2(NO_3)(O_2CEt)_6(bpy)_2](ClO_4)$ (**2**) [40], $[Mn_4O_2(O_2CMe)_7(bpy)_2](ClO_4)$ (**3**) [39] (bpy = 2,2′-bipyridyl), $(NBu^n_4)[Mn_4O_2(O_2CMe)_7(pic)_2]$ (**4**) [36]

Table 2
Selected interatomic distances (Å) and bond angles (°) for $[Mn_4O_2(O_2CEt)_7(bpya)_2](ClO_4)$ (**1**)

Bond lengths			
Mn(2)···Mn(3)	2.871(2)	Mn(3)–O(5)	1.957(3)
Mn(1)–O(5)	1.833(3)	Mn(3)–O(6)	1.876(3)
Mn(1)–O(33)	2.136(3)	Mn(3)–O(40)	1.941(3)
Mn(1)–O(38)	2.107(3)	Mn(3)–O(50)	2.186(3)
Mn(1)–O(43)	1.953(3)	Mn(3)–O(53)	2.134(3)
Mn(1)–N(7)	2.058(4)	Mn(3)–O(58)	2.051(3)
Mn(1)–N(19)	2.087(4)	Mn(4)–O(6)	1.838(3)
Mn(2)–O(5)	1.873(3)	Mn(4)–O(55)	1.948(3)
Mn(2)–O(6)	1.949(3)	Mn(4)–O(60)	2.130(3)
Mn(2)–O(35)	2.047(3)	Mn(4)–O(65)	2.137(3)
Mn(2)–O(45)	2.128(3)	Mn(4)–N(20)	2.035(4)
Mn(2)–O(48)	2.142(3)	Mn(4)–N(32)	2.081(4)
Mn(2)–O(63)	1.937(3)		
Bond angles			
O(33)–Mn(1)–O(38)	93.52(12)	O(5)–Mn(3)–O(53)	99.16(12)
O(33)–Mn(1)–O(43)	92.01(12)	O(5)–Mn(3)–O(58)	172.62(13)
O(5)–Mn(1)–O(33)	93.97(13)	O(6)–Mn(3)–O(40)	173.83(13)
O(5)–Mn(1)–O(38)	175.14(14)	O(6)–Mn(3)–O(50)	87.15(12)
O(5)–Mn(1)–O(43)	90.66(14)	O(6)–Mn(3)–O(53)	88.51(13)
O(5)–Mn(1)–N(7)	173.07(13)	O(6)–Mn(3)–O(58)	99.08(13)
O(5)–Mn(1)–N(19)	91.22(14)	O(40)–Mn(3)–O(50)	98.05(13)
O(33)–Mn(1)–N(7)	88.58(14)	O(40)–Mn(3)–O(53)	86.68(13)
O(33)–Mn(1)–N(19)	86.84(14)	O(40)–Mn(3)–O(58)	84.63(13)
O(38)–Mn(1)–O(43)	92.57(13)	O(50)–Mn(3)–O(53)	172.40(12)
O(38)–Mn(1)–N(7)	85.60(13)	O(50)–Mn(3)–O(58)	86.38(12)
O(38)–Mn(1)–N(19)	88.92(13)	O(53)–Mn(3)–O(58)	88.15(13)
O(43)–Mn(1)–N(7)	90.37(14)	O(6)–Mn(4)–O(55)	94.10(13)
O(43)–Mn(1)–N(19)	175.09(14)	O(6)–Mn(4)–O(60)	93.76(13)
N(7)–Mn(1)–N(19)	85.07(15)	O(6)–Mn(4)–O(65)	91.05(12)
O(5)–Mn(2)–O(6)	82.54(12)	O(6)–Mn(4)–N(20)	176.12(14)
O(5)–Mn(2)–O(35)	98.34(13)	O(6)–Mn(4)–N(32)	91.79(14)
O(5)–Mn(2)–O(45)	88.47(13)	O(55)–Mn(4)–O(60)	94.99(14)
O(5)–Mn(2)–O(48)	88.56(13)	O(55)–Mn(4)–O(65)	92.18(13)
O(5)–Mn(2)–O(63)	174.48(14)	O(55)–Mn(4)–N(20)	89.22(14)
O(6)–Mn(2)–O(35)	172.37(12)	O(55)–Mn(4)–N(32)	173.74(15)
O(6)–Mn(2)–O(45)	100.64(13)	O(60)–Mn(4)–O(65)	171.06(13)
O(6)–Mn(2)–O(48)	87.16(12)	O(60)–Mn(4)–N(20)	83.94(14)
O(6)–Mn(2)–O(63)	94.40(13)	O(60)–Mn(4)–N(32)	86.74(14)
O(35)–Mn(2)–O(45)	86.97(13)	O(65)–Mn(4)–N(20)	90.83(14)
O(35)–Mn(2)–O(48)	85.29(12)	O(65)–Mn(4)–N(32)	85.57(14)
O(35)–Mn(2)–O(63)	85.31(13)	N(20)–Mn(4)–N(32)	84.98(15)
O(45)–Mn(2)–O(48)	171.22(13)	Mn(1)–O(5)–Mn(2)	126.82(16)
O(45)–Mn(2)–O(63)	87.58(13)	Mn(1)–O(5)–Mn(3)	130.10(16)
O(48)–Mn(2)–O(63)	95.90(13)	Mn(2)–O(5)–Mn(3)	97.07(13)
O(5)–Mn(3)–O(6)	82.24(12)	Mn(2)–O(6)–Mn(3)	97.25(13)
O(5)–Mn(3)–O(40)	94.71(12)	Mn(2)–O(6)–Mn(4)	131.38(16)
O(5)–Mn(3)–O(50)	86.43(12)	Mn(3)–O(6)–Mn(4)	125.29(15)

(picH = picolinic acid), $[Mn_4O_2(py)_2(O_2CMe)_6(dbm)_2]$ (**5**) [38] (dbmH = dibenzoylmethane) and $[Mn_4O_2(O_2CPh)_6(dpm)_2]$ (**6**) [47] (dpmH = dipivaloylmethane). All these complexes have idealized C_2 symmetry except for **5**, which possesses a crystallographic inversion center and a planar rather than butterfly Mn_4 topology. The main conclusion to be drawn is that core structures of the C_2 molecules are insignificantly affected by the nature of the chelate ligands and are thus all essentially superimposable, with only minor differences between corresponding structural parameters.

3.3. Magnetochemistry

The molar magnetic susceptibility, χ_m, of complex **1** in the solid state was measured under a constant magnetic field of 1 Tesla in the 5–300 K range. A plot of the effective magnetic moment, μ_{eff}, of complex **1** versus temperature is shown in Fig. 2. The value of μ_{eff} is $8.30\mu_B$ at 300 K and gradually diminishes as the temperature is decreased. A sharp increase of the slope is observed at 50 K, below which μ_{eff} decreases much more rapidly to a value of $4.12\mu_B$ at 5 K.

The Heisenberg spin Hamiltonian for complex **1** is given in Eq. (2), where the numbering in Fig. 1 has been employed.

$$\hat{H} = -2(J_{12}\hat{S}_1\hat{S}_2 + J_{13}\hat{S}_1\hat{S}_3 + J_{23}\hat{S}_2\hat{S}_3 + J_{24}\hat{S}_2\hat{S}_4 + J_{34}\hat{S}_3\hat{S}_4 + J_{14}\hat{S}_1\hat{S}_4) \quad (2)$$

From the virtual C_2 symmetry of **1**, it follows that there are two types of 'body-to-wingtip' Mn–Mn interactions. These can be assumed to be equivalent on the basis of the structural parameters, as was done with previous butterfly complexes, and the spin Hamiltonian then simplifies to that in Eq. (3), where J_{wb} is the wingtip-body interaction, J_{bb} is the body–body interaction,

$$\hat{H} = -2J_{wb}(\hat{S}_1\hat{S}_2 + \hat{S}_1\hat{S}_3 + \hat{S}_2\hat{S}_4 + \hat{S}_3\hat{S}_4) - 2J_{bb}\hat{S}_2\hat{S}_3 - 2J_{ww}\hat{S}_1\hat{S}_4 \quad (3)$$

and J_{ww} refers to the wingtip–wingtip interaction. By use of the Kambe vector coupling method [41,42], and the definitions $\hat{S}_A = \hat{S}_2 + \hat{S}_3$, $\hat{S}_B = \hat{S}_1 + \hat{S}_4$ and $\hat{S}_T = \hat{S}_A + \hat{S}_B$, the spin Hamiltonian can be transformed into that in Eq. (4).

$$\hat{H} = -J_{wb}(\hat{S}_T^2 - \hat{S}_A^2 - \hat{S}_B^2) - J_{bb}\hat{S}_A^2 - J_{ww}\hat{S}_B^2 \quad (4)$$

The corresponding expression of the energy of the spin microstates $|S_T, S_A, S_B\rangle$ is given in Eq. (5). There are a total of 85 S_T states, ranging from $S_T = 0$ to 8.

$$E(S_T, S_A, S_B) = -J_{wb}[S_T(S_T+1) - S_A(S_A+1) - S_B(S_B+1)] - J_{bb}[S_A(S_A+1)] - J_{ww}[S_B(S_B+1)] \quad (5)$$

The solid line in Fig. 2 represents the best fit of the experimental data to the theoretical χ_m versus T equation obtained using the energy values in Eq. (5) and the Van Vleck equation. A temperature independent paramagnetism (TIP) term was held constant at 900×10^{-6} cm^3 mol^{-1}. The fitting parameters were $J_{wb} = -3.27$ cm^{-1}, $J_{bb} = -25.66$ cm^{-1} and $J_{ww} = -0.77$ cm^{-1}, with g held constant at $g = 1.99$. These parameters yield a spin ground state of $S_T = 0$, corresponding to $|0,0,0\rangle$. There is a group of five states, including

Table 3
Comparison of the average core parameters of several $[Mn_4O_2]^{8+}$ complexes (Å, °)

Complex	$Mn_b\cdots Mn_b$	$Mn_b\cdots Mn_w$ [a]	Mn_b–O	Mn_w–O	Mn_b–O–Mn_b	Mn_b–O–Mn_w [a]	O–Mn–O	Dihedral [b]	Ref.
$[Mn_4O_2(NO_3)(O_2CEt)_6(bpy)_2]^+$	2.847	3.258	1.898	1.841	97.2	121.8	82.2	51.80	[40]
		3.344				126.4			
$[Mn_4O_2(O_2CEt)_7(bpya)_2]^+$	2.871	3.307	1.939	1.836	97.16	126.06	82.39	34.69	this work
		3.444				130.74			
$[Mn_4O_2(O_2CMe)_7(bpy)_2]^+$	2.848	3.301	1.912	1.824	96.25	123.7	83.0	44.81	[39]
		3.378				130.2			
$[Mn_4O_2(O_2CMe)_7(pic)_2]^-$	2.842	3.311	1.899	1.844	96.9	125.0	82.1	45.02	[36]
		3.396				129.7			
$[Mn_4O_2(py)_2(O_2CMe)_6(dbm)_2]$	2.875	3.308	1.890	1.877	99.07	123.2	80.93	0.02 [c]	[38]
		3.398				128.6			
$[Mn_4O_2(O_2CPh)_6(dpm)_2]$	2.841	3.255	1.874	1.890	98.53	120.1	81.46	42.0	[47]
		3.362				126.0			

[a] Top and bottom entries refer to Mn pairs bridged by two and one carboxylate, respectively.
[b] Dihedral angle between the two planes formed by the $2Mn_b$ ions with each Mn_w ion.
[c] Planar Mn_4 core.

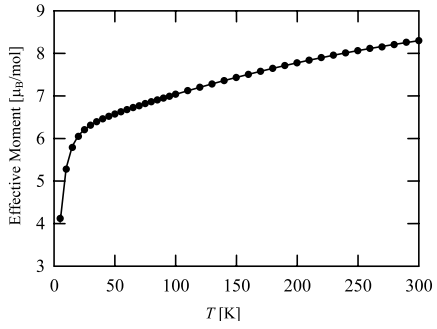

Fig. 2. Plot of effective magnetic moment (μ_{eff}) per molecule vs. T for $[Mn_4O_2(O_2CEt)_7(bpya)_2](ClO_4)$ in a 10.0 kG field. The solid line is a fit of the data to the appropriate theoretical equation; see the text for the fitting parameters.

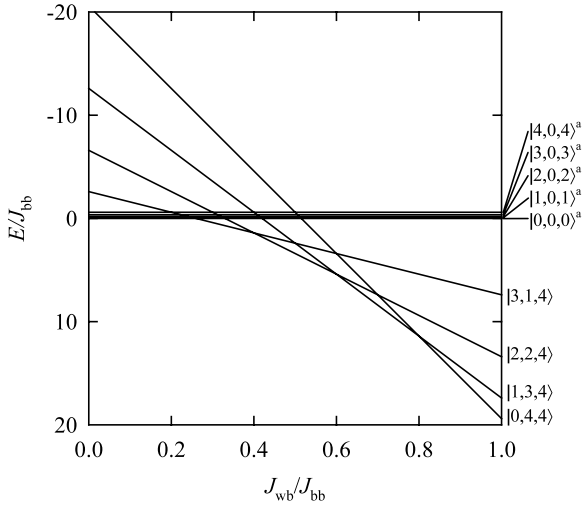

Fig. 3. Relative energy normalized to J_{bb} of the spin-ground state of a $[Mn_4O_2]^{8+}$ system as a function of the ratio J_{wb}/J_{bb} with $J_{ww} = -0.77$ cm^{-1}. For $J_{ww} = 0$, these states would belong to a fivefold degenerate set.

the ground state, within a narrow energy band of 15.3 cm^{-1}, the others being the $|1,0,1\rangle$, $|2,0,2\rangle$, $|3,0,3\rangle$ and $|4,0,4\rangle$ states. This collection of five closely lying spin states becomes degenerate if the weak magnetic coupling between the wing manganese ions (Mn1 and Mn4) is neglected. Although this interaction is very small ($J_{ww} = -0.77$ cm^{-1}), taking it into consideration resulted in a significant improvement of the fit. The introduction of this term results in very small changes to the energies of the different spin states and in the splitting of some groups of states that otherwise would be degenerate, but it strongly influences the behavior of μ_{eff} at very low temperature. The splitting of the ground state caused by this small wing–wing antiferromagnetic interaction leads to a sharp drop of the magnetic moment below 50 K because a diamagnetic state is being populated. Fig. 3 shows the relative energy (normalized to J_{bb}) of the spin ground state for this system as a function of the ratio J_{wb}/J_{bb}, with J_{ww} constant at -0.77 cm^{-1}. This plot shows that the ground-state spin is governed by the J_{wb}/J_{bb} ratio. The value of J_{ww} is assumed to be always very small and it only can affect the ground state when J_{wb}/J_{bb} is sufficiently low, by determining the relative energies of the group of states $|0,0,0\rangle$, $|1,0,1\rangle$, $|2,0,2\rangle$, $|3,0,3\rangle$ and $|4,0,4\rangle$. This is the case in complex **1** ($J_{wb}/J_{bb} = 0.13$), where the drop of μ_{eff} at low temperatures is explained by the existence of the diamagnetic ground state ($|0,0,0\rangle$) that results from the negative value of J_{ww}. A summary of the J_{wb} and J_{bb} parameters found for previously characterized $[Mn_4O_2]^{8+}$ complexes is given in Table 4.

In order to address the question of whether the global rather than a local fitting had been obtained, and to

Table 4
Exchange interaction constants in $[Mn_4O_2]^{8+}$ complexes

Complex	J_{wb} (cm^{-1})	J_{bb} (cm^{-1})	Ref.
$[Mn_4O_2(NO_3)(O_2CEt)_6(bpy)_2]^+$	−1.7	−16.5	[40]
$[Mn_4O_2(O_2CEt)_7(bpya)_2]^+$	−3.3	−25.7	this work
$[Mn_4O_2(O_2CMe)_7(bpy)_2]^+$	−7.8	−23.5	[39]
$[Mn_4O_2(O_2CMe)_7(pic)_2]^-$	−5.3	−24.6	[36]
$[Mn_4O_2(py)_2(O_2CMe)_6(dbm)_2]$	−5.0	−24.9	[38]
$[Mn_4O_2(O_2CPh)_6(dpm)_2]$	−0.4	−27.5	[47]

assess the reliability of the conclusion regarding the ground state of **1**, the relative error surface diagram for this fit was examined. The error surface was generated as a function of J_{wb} (−30.0 to 10.0 cm^{-1}) and J_{bb} (−50.0 to 25.0 cm^{-1}), with J_{ww} and g fixed at −0.77 cm^{-1} and 1.99, respectively. For this, the expression in Eq. (6) was used as the root-mean-square error, where n is the number of data points.

$$\sigma = \sqrt{\frac{\sum(\chi_{calc} - \chi_{exp})^2}{n}} \quad (6)$$

Fig. 4 shows a two-dimensional contour projection of the error surface, showing that the point of minimum error is poorly defined and located within a shallow 'valley'. The area with $\sigma \leq 0.002$ spans approximately the ranges −2 to −4 and −21 to −32 cm^{-1} for J_{wb} and J_{bb}, respectively. Superimposed on top of the contour diagram of Fig. 4 are the lines dividing the {J_{wb}, J_{bb}} space into regions of different ground states. Although the minimum of the error is not very well defined in the surface, it is clear from this plot that the assignment of the spin-ground state is reliable, since the entire region that would contain all reasonable fits is confined within

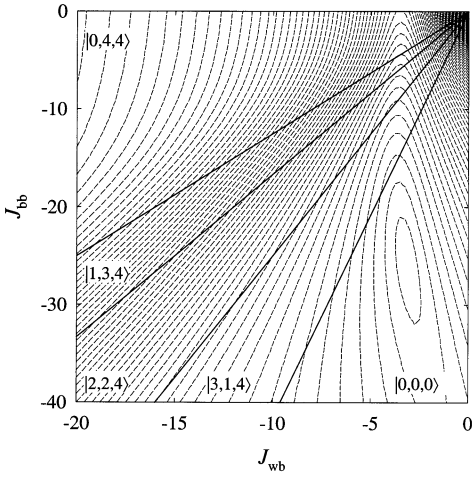

Fig. 4. Error surface of the magnetic susceptibility fit for $[Mn_4O_2(O_2CEt)_7(bpya)_2](ClO_4)$ as a function of J_{wb} and J_{bb}, represented as a contour projection (dashed lines) of the relative error calculated with g and J_{ww} constant at 1.99 and −0.77 cm^{-1}, respectively. Superimposed on the contour diagram are the lines dividing the {J_{wb}, J_{bb}} space into regions of different ground states.

the zone for $S_T = 0$ (or the area where the group of closely lying states |0,0,0⟩, |1,0,1⟩, |2,0,2⟩, |3,0,3⟩, and |4,0,4⟩ have the lowest energy).

The ground state of **1** is in contrast to that of most other $[Mn_4O_2]^{8+}$ complexes [36,38,39] for which the ground state is $S_T = 3$. This emphasizes the importance of the J_{wb}/J_{bb} ratio in determining the ground state of these molecules (Fig. 3). With such a small J_{wb}/J_{bb} ratio (0.13), i.e. $J_{bb} \gg J_{wb}$, the spins of the body Mn ions will be antiparallel-aligned, i.e. $S_A = 0$, and the ground state will then be determined by the interaction of the wingtip Mn ions via the J_{ww} exchange, giving a $S_T = 0$ ground state since J_{ww} is antiferromagnetic. In effect, this |0,0,0⟩ ground state can be described as the result of a weak long-range J_{ww} interaction between the wingtip Mn ions through a strongly coupled, diamagnetic (S_A = 0) central unit. If $J_{ww} = 0$, the ground state is the group of closely spaced states |0,0,0⟩, |1,0,1⟩, |2,0,2⟩, |3,0,3⟩ and |4,0,4⟩, corresponding to two non-interacting Mn(III) ions. The latter situation is approximated in the related complex $[Mn_4O_2(O_2CPh)_6(dpm)_2]$ where the J_{wb}/J_{bb} ratio is only 0.01, J_{ww} is negligible, and the ground state is best described as fivefold degenerate (non-interacting wingtip Mn ions) [47].

3.4. ^1H NMR spectroscopy

Complex **1** is moderately soluble in MeCN and is thus amenable to solution spectroscopic studies. The 500 MHz ^1H NMR spectrum (Fig. 5) was obtained in order to ascertain whether the structure is retained in solution. The spectral data are collected in Table 5. The interpretation of the ^1H NMR spectrum of complex **1** has

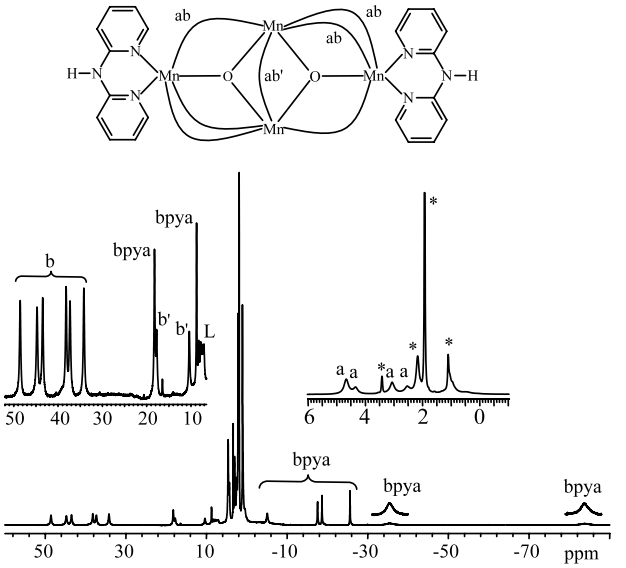

Fig. 5. 500 MHz ^1H NMR spectrum of $[Mn_4O_2(O_2CEt)_7(bpya)_2](ClO_4)$ in CD_3CN; * = $EtCO_2H$, H_2O and MeCN impurities, L = free ligand. Labels a and b refer to propionate CH_3 and CH_2 resonances, respectively.

Table 5
500 MHz ^{1}H NMR data [a] for $[Mn_4O_2(O_2CEt)_7(bpya)_2](ClO_4)$ (**1**) in CD_3CN

a	4.6	bpya	18.3
a	4.3	bpya	8.8
a	3.1	bpya	−5.0
a	2.5	bpya	−17.5
b	48.6(44.7)	bpya	−18.6
b	43.5(38.2)	bpya	−25.5
b	37.3(34.2)	bpya	−35.6
b′	17.8(10.4)	bpya	−83.8

[a] At approximately 23 °C, ppm; *b′* refers to the unique carboxylate bridging the body Mn ions.

benefited from previous spectroscopic studies on the analogous butterfly-like clusters **2**, **3** and **4** [36,39,40].

The ^{1}H NMR spectrum in Fig. 5 exhibits 20 different resonances in addition to the signals from solvent and ligand impurities. This is the number expected if the complex exhibits effective C_2 symmetry in solution. These resonances span a wide range of chemical shifts (−90 to 50 ppm). Four sets of signals in a 2:2:2:1 ratio are observed for the μ_2-O_2CEt groups, according to the scheme shown in Fig. 5. Each of these sets features two peaks from the CH_2 protons, which are diastereotopic, in the 10–50 ppm region, and a singlet from the CH_3 group between 2 and 5 ppm. The two chelating ligands are symmetry-related but all the protons within each bpya group are inequivalent. Accordingly, eight bpya signals are observed, and these display great disparity of linewidths as a result of their different separations from the Mn ions (broadness $\propto r^{-6}$, where r is the Mn···H distance). In addition, these eight resonances are subject to strong paramagnetic shifts to either side of the diamagnetic region, indicating that a π spin-delocalization mechanism is contributing to the coupling of the nuclear and electronic magnetic moments. All these results indicate that the structure of **1** in the solid state is retained in MeCN solution. In contrast, when the cluster is dissolved in DMSO, decomposition takes place, as is evident from the complete loss of the ^{1}H NMR spectral features in this solvent.

3.5. Electrochemistry

Complex **1** was investigated by cyclic voltammetry in MeCN solution with 0.1 M $N^nBu_4PF_6$. The voltammogram of this compound at a scan rate of 100 mV s^{-1} is displayed in Fig. 6. This complex shows a quasi-reversible oxidation process and an irreversible reduction process at 0.71 and −0.20 V versus Fc/Fc^+, respectively. The quasi-reversible oxidation has a peak-to-peak separation of 130 mV and is likely metal-based (Eq. (7)).

$$[Mn_4^{III}O_2]^{8+} - e^- \rightarrow [Mn_3^{III}Mn^{IV}O_2]^{9+} \quad (7)$$

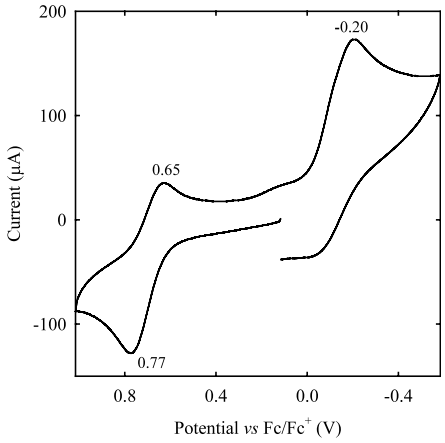

Fig. 6. Cyclic voltammogram at 100 mV s^{-1} for $[Mn_4O_2(O_2CEt)_7(bpya)_2](ClO_4)$ in MeCN containing 0.1 M $NBu^n_4PF_6$.

These values are similar to what has been observed previously for the $[Mn_4O_2(O_2CR)_7(L–L)]^+$ (R = Me, Ph; L–L = bpy, phen, 4-4′-Me_2-bpy) complexes reported previously by our group. Thus the non-ligation to Mn of the NH group of bpya results in **1** exhibiting very similar redox properties to the corresponding bpy and phen complexes.

4. Conclusions

The new tetranuclear complex $[Mn_4O_2(O_2CEt)_7(bpya)_2](ClO_4)$ (**1**) forms from the comproportionation reaction between Mn^{II} and Mn^{VII} in propionic acid in the presence of bpya. The title compound is the first crystallographically characterized species containing the ligand bpya bound to manganese. Unlike the majority of previously characterized Mn clusters with a butterfly core, complex **1** possesses a spin ground state of $S_T = 0$. This result emphasizes that only small changes in the relative strength of competing exchange interactions are necessary in a $[Mn_4O_2]^{8+}$ butterfly system for a change of the ground state spin value to occur. ^{1}H NMR spectroscopy has shown that the new complex retains its structure in MeCN solution. Complex **1** is a new addition to the list of crystallographically characterized clusters with the $[Mn_4O_2]^{8+}$ core.

5. Supplementary material

Crystallographic data for the structural analysis have been deposited with the Cambridge Crystallographic Data Centre, CCDC No. 175700 for compound **1**. Copies of this information may be obtained free of charge from The Director, CCDC, 12 Union Road, Cambridge, CB2 1EZ, UK (fax: +44-1223-336033; e-

mail: deposit@ccdc.cam.ac.uk or www: http://www.ccdc.cam.ac.uk) [48].

References

[1] V.L. Pecoraro (Ed.), Manganese Redox Enzymes, VCH Publishers, New York, 1992.
[2] H.J. Eppley, H.-L. Tsai, N. de Vries, K. Folting, G. Christou, D.N. Hendrickson, J. Am. Chem. Soc. 117 (1995) 301.
[3] G. Aromí, S.M.J. Aubin, M.A. Bolcar, G. Christou, H.J. Eppley, K. Folting, D.N. Hendrickson, J.C. Huffman, R.C. Squire, H.-L. Tsai, S. Wang, M.W. Wemple, Polyhedron 17 (1998) 3005.
[4] S.M.J. Aubin, M.W. Wemple, D.M. Adams, H. -L. Tsai, G. Christou, D.N. Hendrickson, J. Am Chem. Soc. 118 (1996) 7746.
[5] S.M.J. Aubin, N.R. Dilley, M.W. Wemple, M.B. Maple, G. Christou, D.N. Hendrickson, J. Am Chem. Soc. 120 (1998) 839.
[6] S.M.J. Aubin, S. Spagna, H.J. Eppley, R.E. Sager, K. Folting, G. Christou, D.N. Hendrickson, Mol. Cryst. Liq. Cryst. 305 (1997) 181.
[7] H. -L. Tsai, S. Wang, K. Folting, W.E. Streib, G. Christou, D.N. Hendrickson, J. Am. Chem. Soc. 117 (1995) 2503.
[8] H.J. Eppley, S. Wang, H. -L. Tsai, S.M.J. Aubin, K. Folting, W.E. Streib, G. Christou, D.N. Hendrickson, Mol. Cryst. Liq. Cryst. 274 (1995) 159.
[9] G. Christou, in: O. Kahn (Ed.), Magnetism: a Supramolecular Function, NATO ASI Series, Kluwer, Dordrecht, 1996.
[10] M.A. Bolcar, S.M.J. Aubin, K. Folting, D.N. Hendrickson, G. Christou, J. Chem. Soc., Chem. Commun. (1997) 1485.
[11] G. Aromí, M.J. Knapp, J.-P. Claude, J.C. Huffman, D.N. Hendrickson, G. Christou, J. Am. Chem. Soc. 121 (1999) 5489.
[12] R. Sessoli, H. -L. Tsai, A.R. Shake, S. Wang, J.B. Vincent, K. Folting, D. Gatteschi, G. Christou, D.N. Hendrickson, J. Am. Chem. Soc. 115 (1993) 1804.
[13] R. Sessoli, D. Gatteschi, A. Caneschi, M.A. Novak, Nature 365 (1993) 141.
[14] J.R. Friedman, M.P. Sarachik, J. Tejada, J. Maciejewski, R. Ziolo, J. Appl. Phys. 79 (1996) 6031.
[15] J. Tejada, R.F. Ziolo, X.X. Zang, Chem. Mater. 8 (1996) 1784.
[16] J.M. Hernádez, X.X. Zang, F. Luis, J. Bartolomé, J. Tejada, R. Ziolo, Europhys. Lett. 35 (1996) 301.
[17] A.L. Barra, P. Debrunner, D. Gateschi, C.E. Shultz, R. Sessoli, Europhys. Lett. 35 (1996) 133.
[18] H.J. Eppley, N. de Vries, S. Wang, S.M.J. Aubin, K. Folting, D.N. Hendrickson, G. Christou, Inorg. Chim. Acta 263 (1997) 323.
[19] M.W. Wemple, H. -L. Tsai, S. Wang, J. -P. Claude, W.E. Streib, K. Folting, G. Christou, Inorg. Chem. 35 (1996) 6437.
[20] H.J. Eppley, S.M.J. Aubin, W.E. Streib, J.C. Bollinger, D.N. Hendrickson, G. Christou, Inorg. Chem. 36 (1997) 109.
[21] R.C. Squire, S.M.J. Aubin, K. Folting, W.E. Streib, G. Christou, D.N. Hendrickson, Inorg. Chem. 34 (1995) 6463.
[22] M.A. Halcrow, W.E. Streib, K. Folting, G. Christou, Acta Crystallogr., Sect.C C51 (1995) 1263.
[23] S. Wang, H. -L. Tsai, K.S. Hagen, D.N. Hendrickson, G. Christou, J. Am. Chem. Soc. 116 (1994) 9339.
[24] D. Luneau, J. -M. Savarinult, J. -P. Tuchagues, Inorg. Chem. 27 (1988) 3912.
[25] R. Bhula, D.C. Weatherburn, Angew. Chem., Int. Ed. Engl. 30 (1991) 688.
[26] D.W. Low, D.M. Eichhorn, A. Draganescu, W.H. Armstrong, Inorg. Chem. 30 (1991) 877.
[27] G.A. Bowmaker, P.C. Healy, D.L. Kepert, J.D. Kildea. B.W. Skelton, A.H. White, J. Chem. Soc., Dalton Trans. (1989) 1639.
[28] O.R. Rodig, T. Brueckner, B.H. Hurlburt, R.K. Schlatzer, T.L. Venable, E. Sinn, J. Chem. Soc., Dalton Trans. (1981) 196.
[29] N.J. Ray, L. Hulett, R. Sheahan, B.J. Hathaway, J. Chem. Soc., Dalton Trans. (1981) 1463.
[30] N. Marsich, A. Camus, F. Ugozzoli, A.M.M. Lanfredi, Inorg. Chim. Acta 236 (1995) 117.
[31] L.-P. Wu, M.E. Keniry, B. Hathaway, Acta Crystallogr., Sect. C. (Cr. Str. Commun.) 48 (1992) 35.
[32] L.-P. Wu, P. Field, T. Morrissey, C. Murphy, P. Nagle, B. Hathaway, C. Simmons, P. Thornton, J. Chem. Soc., Dalton Trans. (1990) 3835.
[33] F.A. Cotton, L.M. Daniels, C.A. Murillo, I. Pascual, Inorg. Chem. Commun. 1 (1998) 1.
[34] E-C. Yang, M.-C. Cheng, M.-S. Tsai, S.-M. Peng, J. Chem. Soc., Chem. Commun. (1994) 2377.
[35] S. Wang, H.-L. Tsai, W.E. Streib, G. Christou, D.N. Hendrickson, J. Chem. Soc., Chem. Commun. (1992) 677.
[36] E. Libby, J.K. McCusker, E.A. Schmitt, K. Folting, D.N. Hendrickson, G. Christou, Inorg. Chem. 30 (1991) 3486.
[37] E. Bowman, M.A. Bolcar, E. Libby, J.C. Huffman, K. Folting, G. Christou, Inorg. Chem. 31 (1992) 5185.
[38] S. Wang, K. Folting, W.E. Streib, E.A. Schmitt, J.K. McCusker, D.N. Hendrickson, G. Christou, Angew. Chem., Int. Ed. Engl. 30 (1991) 305.
[39] J.B. Vincent, C. Christmas, H. -R. Chang, Q. Li, P.D.W. Boyd, J.C. Huffman, D.N. Hendrickson, G. Christou, J. Am. Chem. Soc. 111 (1989) 2086.
[40] G. Aromí, S. Bhaduri, P. Artús, K. Folting, G. Christou, Inorg. Chem. 41 (2002) 805.
[41] K. Kambe, J. Phys. Soc. Jpn. 5 (1950) 8.
[42] A. Cornia, D. Gatteschi, K. Hegetschweiler, Inorg. Chem. 33 (1994) 1559.
[43] A.J. Blake, S. Parsons, J.M. Rawson, R.E.P. Winpenny, Polyhedron 14 (1995) 1895.
[44] F.A. Cotton, L.M. Daniels, G.T Jordan, IV, C.A. Murillo, J. Am. Chem. Soc. 119 (1997) 10377.
[45] G. Christou, Acc. Chem. Res. 22 (1989) 328.
[46] (a) J.B. Vincent, K Folting, J.C. Huffman, G. Christou, Inorg. Chem. 24 (1986) 996;
(b) J.B. Vincent, H. -R Chang, K. Folting, J.C. Huffman, G. Christou, D.N. Hendrickson, J. Am. Chem. Soc. 109 (1987) 5703.
[47] C. Cañada- Vilalta, J.C. Huffman, G. Christou, Polyhedron 20 (2001) 1785.
[48] F.H. Allen, O. Kennard, Chem. Des. Automation News 8 (1993) 131 (The Cambridge Structural Database).